Numerical Study of Multi-Dimensional Liquid-Fuel n-Dodecane/Air Detonations with Complex Chemistry

Sai Sandeep Dammati[1], Yoram Kozak[2], Alexei Poludnenko[3,1]

[1]Department of Aerospace Engineering, Texas A&M University
College Station, TX, USA
[2] School of Mechanical Engineering, University of Tel-Aviv
Tel-Aviv, Israel
[3]Department of Mechanical Engineering, University of Connecticut
Storrs, CT, USA

1 Introduction

Detonations in liquid fuel sprays play a crucial role for the development of the novel detonation-based propulsion and energy conversion systems such as Rotating Detonation Engines (RDEs) due to a number of practical advantages presented by liquid fuels compared to gas-phase ones such as hydrogen, methane, or ethylene, which are currently used in RDE research. Furthermore, understanding of detonation dynamics in sprays is important for prevention and mitigation of industrial accidents, as well as for various munitions applications. Over the past two decades, significant emphasis has been placed on studying multi-dimensional single-phase gaseous detonations [1–3]. Even though those efforts have resulted in significant advances of our understanding of the structure and dynamics of detonations in different mixtures, it is not clear to what extent these insights are applicable to multi-phase detonations. The presence of a liquid spray, especially without any prevaporized ambient fuel, brings in qualitatively different effects associated with flow-droplet interactions, droplet secondary atomization, evaporative cooling, vaporization and mixing. All these processes affect both the spray and the ambient flow resulting in complex mass, momentum, and energy exchange and ultimately in mass loading of the flow and subsequent fuel mixing with the oxidizer, which are critical for the sustained detonation propagation. All these additional complexities can significantly alter the detonation structure and they can directly impact its stability and propagation limits in liquid sprays.

In comparison to gas-phase detonations, the field of liquid-fuel detonations is relatively less developed despite a number of theoretical and experimental studies over the past 60 years [4, 5]. In particular, several analytical and semi-analytical spray detonation models [6–8] were proposed, which are limited to one-dimensional systems. In terms of two-dimensional spray detonations, several studies have been presented in recent years, though typically they are restricted to simplified two-step or tabulated chemistry. For instance, Cheatham et. al. [9] and Schwer et. al. [10] studied detonations in JP10/O_2 mixtures modelled using calibrated two-step chemistry. Zhao et. al. [11] recently studied spray detonations in n-heptane/air mixtures using a two-step chemistry model in OpenFoam.

In this study, we present the results of a two-dimensional simulation of a spray detonation in n-dodecane/air using complex multi-step chemical kinetics and state-of-the-art droplet drag and evaporation models. To

Correspondence to: saisandeepdammati@tamu.edu

the authors' knowledge, this is the first such study of a spray detonation in a heavy hydrocarbon fuel using multi-step chemistry.

2 Numerical Method and Problem Setup

In the current work, numerical simulations involve a coupled gas-particle system that is solved via a Eulerian-Lagrangian approach. The governing equations are the two-dimensional unsteady compressible reactive Navier-Stokes equations for the gas phase in the Eulerian frame of reference coupled with the Lagrangian droplet equations for the dynamics of the liquid phase. The governing equations for the gas phase are:

$$\frac{\partial \rho_g}{\partial t} + \nabla \cdot (\rho_g \mathbf{U}_g) = S_\rho, \tag{1}$$

$$\frac{\partial \rho_g \mathbf{U}_g}{\partial t} + \nabla \cdot (\rho_g \mathbf{U}_g \otimes \mathbf{U}_g) + \nabla P_g = \nabla \cdot \Pi + \mathbf{S}_M, \tag{2}$$

$$\frac{\partial E_g}{\partial t} + \nabla \cdot ((E_g + P_g)\mathbf{U}_g) - \nabla \cdot (K_g \nabla T_g - \rho h_k D_k) = \rho_g \Delta h_{f,k} \dot{w}_k + \nabla \cdot (\Pi \cdot \mathbf{U}_g) + S_E, \tag{3}$$

$$\frac{\partial \rho_g Y_k}{\partial t} + \nabla \cdot (\rho_g Y_k \mathbf{U}_g) - \nabla \cdot (D_k \nabla Y_k) = \rho_g \dot{w}_k + S_{Y,f}, \tag{4}$$

where t is time, ρ_g is the gas density, $\mathbf{U}_g$ is the gas velocity vector, P_g is pressure, E_g is the total energy density, T_g is the gas temperature, K_g and D_g are the thermal and mass diffusion coefficients of the gas. Y_k, $\Delta h_{f,k}$ and $\dot{w}_k$ are the mass fraction, specific enthalpy of formation and the net production rate of the k-th species, respectively. Π is the viscous stress tensor, which is given by the following relation:

$$\Pi = \mu(\nabla \mathbf{U}_g + (\nabla \mathbf{U}_g)^T) + (\mu_B - \frac{2}{3}\mu)(\nabla \cdot \mathbf{U}_g)\mathbf{I}, \tag{4}$$

where μ and μ_B are the dynamic shear viscosity and bulk viscosity of the gas respectively and $\mathbf{I}$ is the identity matrix. S_ρ, $\mathbf{S}_M$, S_E and $S_{Y,f}$ are source terms for the exchange of mass, momentum, energy and fuel mass fraction, respectively, between the particles and the gas. The droplets are represented in a Lagrangian frame of reference. Accordingly, for each particle, the following equations are solved:

$$\frac{d\mathbf{x}_p}{dt} = \mathbf{v}_p \qquad \frac{d\mathbf{v}_p}{dt} = \frac{\mathbf{U}_g - \mathbf{v}_p}{\tau_s} \qquad \frac{dm_p}{dt} = \frac{m_p}{\tau_m} \qquad \frac{dT_p}{dt} = \frac{(T_g - T_p - \frac{2L_v e^\beta - 1}{c_{p,f}})}{\tau_t},$$

where $\mathbf{x}_p$ is the particle position, $\mathbf{v}_p$, T_p are the particle velocity and temperature, respectively, m_p is the particle mass, $c_{p,p}$ is the particle specific heat capacity, and τ_s, τ_m, and τ_t are the characteristic momentum, mass, and heat transfer time scales of the droplet, respectively, which are given by the following relations:

$$\tau_s = \frac{4}{3}\frac{\rho_p}{\rho_f}\frac{a}{C_d}\frac{1}{|\mathbf{U}_g - \mathbf{v}_p|} \qquad \tau_m = \frac{a^2 \rho_p}{6 Sh D_f \rho_f ln[1 + B_{m,neq}]} \qquad \tau_t = \frac{2\tau_m (e^\beta - 1) c_{p,p} \rho_p}{Nu c_{p,f}}.$$

Here a and ρ_p are the particle diameter and density, respectively, C_d is the drag coefficient, Nu is the Nusselt number, L_v is the latent heat of vaporization, and $c_{p,f}$, D_f, and ρ_f are the gas specific heat capacity, mass diffusivity, and density in the film. Sh is the Sherwood number, $B_{m,neq}$ is the non-equilibrium Spalding mass transfer number and β is the non-dimensional evaporation parameter.

The equations are solved with `Athena-RFX`, which is a fully compressible multi-phase reacting flow solver [13–15]. The solver is based on a directionally unsplit high-order Godunov method with piecewise-linear method for spatial reconstruction of interface states and HLLC-ADC Riemann solver [16]

to compute the interface fluxes. YASS ODE integrator is used to solve the stiff system of equations for chemical kinetics, and the chemistry is coupled to the flow equations using Strang splitting [17]. The equation of state is that of an ideal gas with the thermodynamic functions computed using NASA seven-coefficient format. The molecular transport coefficients are evaluated using mixture averaging.

For droplets, the Crank-Nicolson method is used for integration. Note that droplets are two-way coupled to the flow equations, thus the coupling is based on a predictor-corrector scheme [20]. This coupling approach provides 2^{nd}-order temporal accuracy and guarantees mass, momentum, and energy conservation up to machine accuracy for the entire gas-particle system. Interpolation of flow quantities to a particle position is performed using WENO-5 weight function [14]. The particle-gas interaction includes quasi-steady drag and forced convective heat transfer. As particles are assumed to be perfectly spherical, the drag coefficient is evaluated with the correlation of Loth [18] for high-speed regimes, and the Nusselt and Sherwood numbers are given by the Ranz-Marshall correlation [19]. Mass, momentum, and energy source terms, which represent the particle-gas interaction, are spread from the particles back to the grid via a 5-point stencil high-order B-spline weight function [21]. Note that droplet-droplet interactions are not included under the assumption of a dilute spray and we assume constant liquid properties. Further, secondary atomization of the liquid droplets is not considered due to the 2D nature of the simulation. Finally, pyrolysis and oxidation of n-dodecane in the gas-phase is described by a 24-species reduced reaction model developed using HyChem approach [12, 23].

The numerical simulation is carried out in a 2D rectangular channel 64 cm long in the streamwise direction and 10 cm wide in the transverse direction. Initially, the left half of the domain is filled with air at 1 bar, 420 K while the right half of the domain is filled with hot air with temperature and pressure corresponding to the von Neumann (post-shock) state of an equivalent 1D purely gaseous n-dodecane/air detonation. The interface (shock) separating these two regions of air is sinusoidally perturbed to initialize transverse motion. The computational cell size is set to 42 μm, which corresponds to 40 cells per induction length and roughly 6 cells per exothermic pulse width in the ZND solution of an equivalent purely gaseous n-dodecane/air detonation. The right boundary is held constant at the Chapman-Jouguet (CJ) state of an equivalent purely gaseous detonation. 10 μm size liquid dodecane droplets at a temperature of 300 K are injected from the left boundary of the domain at CJ velocity $D_{CJ} = 1792$ along with air at 420 K. Under these conditions, droplet pre-vaporization before they enter the detonation front is minimal. The initial inter-droplet separation is ≈ 4.5 computational cells. This droplet seeding density is chosen such that stoichiometric n-dodecane/air mixture is produced if droplets are completely evaporated and mixed with air. Adiabatic, slip walls are used in the transverse direction to avoid any momentum and heat losses in the channel, and the problem is solved in the shock frame of reference. The simulation is carried out until the detonation propagates a distance of 15 domain widths or $\approx$ 1.5 m.

3 Results and Discussion

We find that toward the end of our simulation, the detonation wave speed, D, in our spray-supported system approaches the gaseous CJ detonation velocity $D_{CJ} = 1792$ m/s. Initially, the detonation velocity drops significantly as there is no fuel present in the gas phase to support chemical heat release, which ultimately controls the detonation wave speed. As the initial shock perturbation collapses and droplets begin to move into the shock and evaporate, the detonation speed begins to increase. Droplets that cross the shock first begin to evaporate rapidly and this produces several local reactive regions, which create local blasts that initially over-drive the detonation. With time, droplets start to evaporate at a much more regular rate, which stabilizes the detonation velocity close to D_{CJ}. We observe a similar behavior in our 1D simulations as well (not shown here). The fact that both purely gaseous and spray detonations propagate with the same speed is expected based on prior theoretical studies [8]. After all droplets have

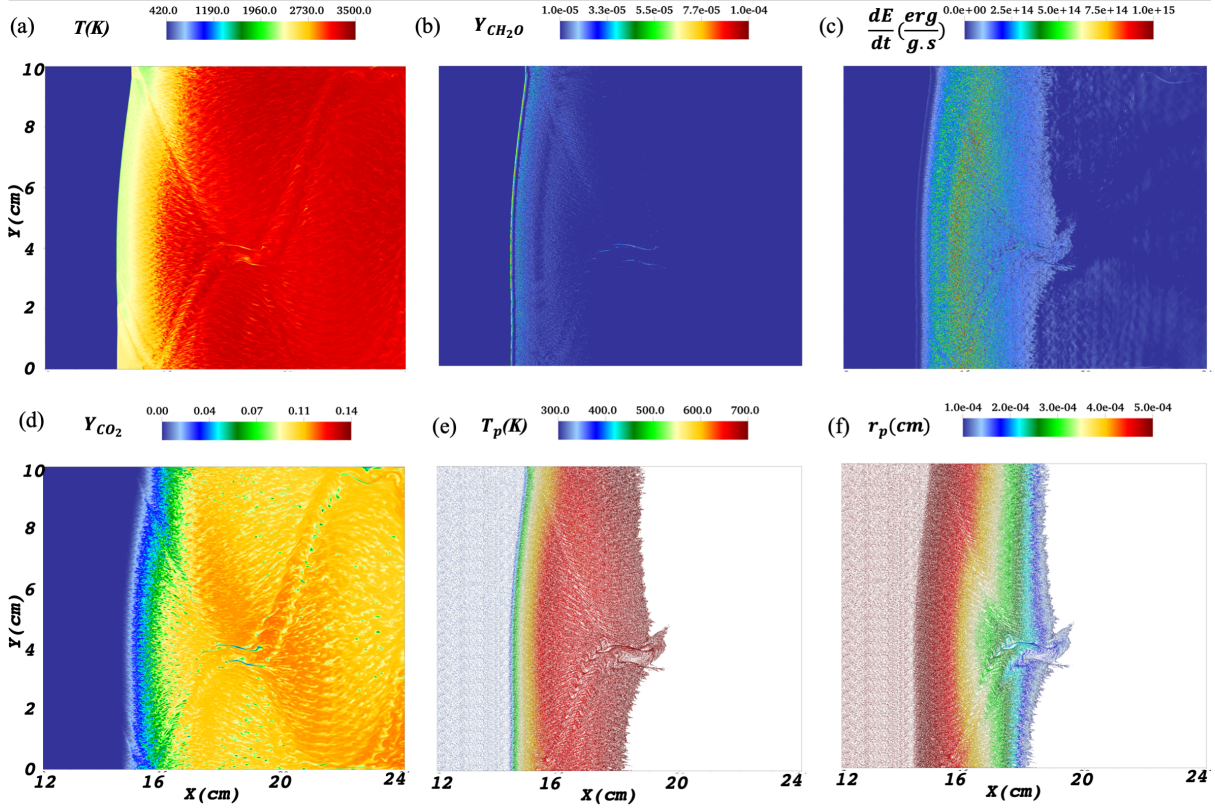

Figure 1: Structure of a 2D spray detonation in a stoichiometric $nC_{12}H_{26}$/air mixture. Panels (a), (b), (c), (d) show the temperature, CH_2O mass fraction, heat release rate, and CO_2 mass fraction. Panels (e) and (f) show the temperature and radius of liquid droplets.

evaporated, the heat release in both gaseous and spray detonation systems for the same equivalence ratio will be the same and therefore, the detonation wave speed is also expected to remain the same. Similar observation of the detonation wave speed was also made in previous studies [9, 10]. Note that energy expended to evaporate the droplets is small relative to the chemical energy release in the front and thus it has a negligible effect on the detonation velocity.

Figure 1 shows the structure of the 2D spray detonation. Panels a and d show the presence of transverse waves along the detonation front. The heat release rate (Fig. 1c) indicates that the induction length and exothermic pulse width are both on the order of a few cm and they are significantly larger than those predicted by the ZND theory for gas-phase n-dodecane/air detonations at 1 bar, 420 K and ϕ = 1.0, namely 1.7 and 0.25 mm, respectively. The droplet temperature and radius distribution is shown in Figs.1e and 1f respectively. As expected, droplets begin to heat up immediately after they cross the shock and they reach temperatures above 650 K (close to their boiling point at the post-shock pressures) over a short distance. At the same time, the radius of droplets starts to decrease much more gradually further downstream. This is a typical characteristic of a non-volatile heavy hydrocarbon fuel such as n-dodecane, which results in a relatively slow mass loading of the flow due to evaporation over a large distance thus leading to an extended reaction zone.

Finally, Figure 2 shows the numerical soot foil obtained by recording the maximum pressure in each computational cell in the domain. It can be seen that the initial collapse of the perturbed shock leads to the formation of several transverse waves. However, as the simulation proceeds, only one dominant pressure mode emerges resulting in a single-headed detonation with cell length ≈ 45 cm, which propagates over a distance from $\approx$ 600 to 550 cm. After that, a second transverse wave appears in the domain,

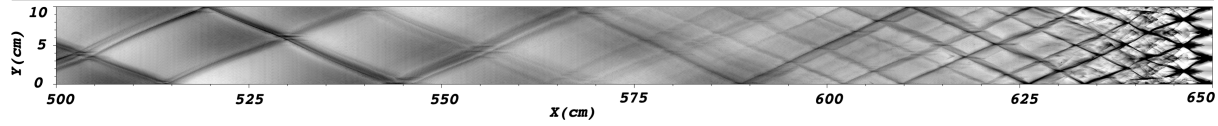

Figure 2: Numerical soot foil obtained by recording the maximum pressure in each computational cell.

and together these two transverse waves form a single-detonation cell, with cell width equal to the domain width of 10 cm and cell length of $\approx$ 20 cm. Since there is no experimental data available on the cell size of purely gaseous n-dodecane/air mixtures at the conditions studied, a direct comparison of cell sizes is not possible here. Based on the induction length scaling arguments for gas-phase detonations in heavy hydrocarbons [22], for the conditions of 1 bar, 420 K and ϕ = 1.0, the expected cell width for a purely gas-phase detonation is $\approx$ 4 cm. If we consider this cell size of 4 cm to be correct, then we observe a significantly larger cell size in the equivalent liquid-fuel detonation. This increase in cell size can be attributed to the fact that the induction and exothermic zone lengths in the spray detonation system are both much larger than the values predicted by the ZND theory for purely gas-phase detonations. Since the detonation cell size increases with the induction length, we observe a larger detonation cell size. We note though that this particular cell size of 10 cm may still be mode-locked due to a relatively small channel width and significantly wider channels must be considered in future work.

Before we conclude, we emphasize that our 2D simulations do not include secondary atomization, which is expected to play an important role in liquid-fuel detonations. In particular, it can severely alter the induction and exothermic lengths, which in turn would modify the entire detonation structure and dynamics. A 3D spray detonation with secondary atomization would be a more realistic configuration to study, however, such a calculation requires extremely large computing resources with accurate secondary atomization models for detonations. Such calculation is currently underway and it will be presented elsewhere.

4 Acknowledgements

SSD and AYP acknowledge funding support through the Air Force Office of Scientific Research (AFOSR) under Grant FA9550-21-1-0012 (Program Manager: Dr. Chiping Li). Computing resources are provided in part by the DoD High Performance Computing Modernization Program.

References

[1] Taylor BD, Kessler DA, Gamezo VN, Oran ES. Numerical simulations of hydrogen detonations with detailed chemical kinetics. Proc. Comb. Inst. 2013 Jan 1;34(2):2009-16.

[2] Tsuboi N, Katoh S, Hayashi AK. Three-dimensional numerical simulation for hydrogen/air detonation: Rectangular and diagonal structures. Proc. Comb. Inst. 2002 Jan 1;29(2):2783-8.

[3] Gamezo VN, Vasil'ev AA, Khokhlov AM, Oran ES. Fine cellular structures produced by marginal detonations. Proceedings of the Combustion Institute. 2000 Jan 1;28(1):611-7.

[4] Bar-Or R, Sichel M, Nicholls JA. The propagation of cylindrical detonations in monodisperse sprays. Proc. Comb. Inst. 1981 Jan 1 (Vol. 18, No. 1, pp. 1599-1606). Elsevier.

[5] Kailasanath K. Liquid-fueled detonations in tubes. Journal of Propulsion and Power. 2006 Nov;22(6):1261-8.

[6] Williams FA. Structure of detonations in dilute sprays. The Physics of Fluids. 1961 Nov;4(11):1434-43.

[7] Gubin SA, Sichel M. Calculation of the detonation velocity of a mixture of liquid fuel droplets and a gaseous oxidizer. Combustion Science and Technology. 1977 Dec 1;17(3-4):109-17.

[8] Lu T, Law CK. Heterogeneous effects in the propagation and quenching of spray detonations. Journal of propulsion and power. 2004 Sep;20(5):820-7.

[9] Cheatham S, Kailasanath K. Numerical modelling of liquid-fuelled detonations in tubes. Combustion Theory and Modelling. 2005 Feb 1;9(1):23-48.

[10] Schwer DA. Multi-dimensional Simulations of Liquid-Fueled JP10/Oxygen Detonations. InAIAA Propulsion and Energy 2019 Forum 2019 (p. 4042).

[11] Zhao M, Zhang H. Numerical simulation of two-dimensional detonation propagation in partially pre-vaporized n-heptane sprays. arXiv preprint arXiv:2103.12525. 2021 Mar 23.

[12] Gao Y, Shan R, Lyra S, Li C, Wang H, Chen JH, Lu T. On lumped-reduced reaction model for combustion of liquid fuels. Combustion and Flame. 2016 Jan 1;163:437-46.

[13] Poludnenko AY, Oran ES. The interaction of high-speed turbulence with flames: Global properties and internal flame structure. Combustion and Flame. 2010 May 1;157(5):995-1011.

[14] Kozak Y, Dammati SS, Bravo LG, Hamlington PE, Poludnenko AY. WENO interpolation for Lagrangian particles in highly compressible flow regimes. Journal of Computational Physics. 2020 Feb 1;402:109054.

[15] Dammati SS, Kozak Y, Rising C, Reyes J, Ahmed KA, Poludnenko AY. Numerical investigation of the accuracy of particle image velocimetry technique in gas-phase detonations. Proceedings of the Combustion Institute. 2021 Jan 1;38(3):3671-81.

[16] Simon S, Mandal JC. A cure for numerical shock instability in HLLC Riemann solver using antidiffusion control. Computers & Fluids. 2018 Sep 30;174:144-66.

[17] Strang G. On the construction and comparison of difference schemes. SIAM journal on numerical analysis. 1968 Sep;5(3):506-17.

[18] Loth E. Compressibility and rarefaction effects on drag of a spherical particle. AIAA journal. 2008 Sep;46(9):2219-28.

[19] Edi SE, On TI, Crowe CT, Schwarzkopf JD, Sommerfeld M, Tsuji Y. Multiphase flows with droplets and particles.

[20] Bai XN, Stone JM. Particle-gas dynamics with Athena: method and convergence. The Astrophysical Journal Supplement Series. 2010 Sep 20;190(2):297.

[21] Abe H, Sakairi N, Itatani R, Okuda H. High-order spline interpolations in the particle simulation. Journal of computational physics. 1986 Apr 1;63(2):247-67.

[22] Tieszen SR, Stamps DW, Westbrook CK, Pitz WJ. Gaseous hydrocarbon-air detonations. Combustion and Flame. 1991 Apr 1;84(3-4):376-90.

[23] Xu, C., Poludnenko, A.Y., Zhao, X., Wang, H., Lu, T., Structure of strongly turbulent premixed n-dodecane–air flames: Direct numerical simulations and chemical explosive mode analysis. Combustion and Flame. 2019; 209:27-40.